TEST Engineering & Management

March - April 2020
ISSN: 0193-4120 Page No. 7984 - 7992

Automatic Framework for the Detection of Coronary Artery Calcification in IVUS Images

S.Mohammad[1], H.Sofian [2], N.M.Noor[3]

[1]Universiti Kuala Lumpur - British Malaysian Institute, Gombak Selangor
[2]Universiti Kuala Lumpur - Malaysian Institute of Information Technology, Kuala Lumpur
[3]UTM Razak School of Engineering and Advanced Technology, UniversitiTeknologi Malaysia (UTM), Kuala Lumpur
[1]surayamohamad@unikl.edu.my

Article Info
Volume 83
Page Number: 7984 - 7992
Publication Issue:
March - April 2020

Article History
Article Received*: 24 July 2019*
Revised*: 12 September 2019*
Accepted*: 15 February 2020*
Publication*: 09 April 2020*

Abstract

The paper propose an automatic framework for the detection of coronary artery calcification in intravascular ultrasound (IVUS) images using texture analysis method. The texture features used is called Histogram of Equivalent Patterns (HEPs) Features. Experiments was conducted using 2175 IVUS images, 530 with calcification plague and 1645 without calcification plague. The images are from dataset B of MICCAI challenge 2011. The classifier used is 1-NN classifier. A 2-fold cross-validation process is applied to the IVUS image database to evaluate the performance of the proposed framework. The highest accuracy obtained is 95.89 %, using a variant of Com-pleted Local Binary Patterns (CLBP) descriptors as the features.

Index Terms; *Intravascular ultrasound image, image classifi-cation, HEP features, Calcification in IVUS image*

I. INTRODUCTION

According to a report by WHO, Cardiovascular Disease (CVD) is the leading of non-communicable diseases (NCDs) that causes death. It was estimated in 2016 that around, 41 million death are caused by the NCDs which is equivalent to 71% of all deaths globally. Out of this 17.9 million deaths (44 %) are due to CVD, 9.0 million deaths (22%) are due to cancer, 3.8 million deaths (9%) are due to chronic respiratory disease and 1.6 million deaths (4%) are due to diabetes [1].

Cardiovascular Disease includes numerous problems, and of them is Coronary artery disease (CAD). Most often Coronary artery disease is related to a process called Atherosclerosis, a disease of the vessel wall. Atherosclerosis develops when plaque started to builds up in the artery wall. This buildup narrows the arteries, causing it harder for blood to flow through the artery. If the accumulated plague is ruptured, the blood will clot inside the artery and this can prevent the blood flow, which then may lead to heart attack or stroke.

A number of imaging modalities exist to the assist di-agnosing the coronary artery diseases. The most commonly used diagnostic tools are X-ray coronary angiography and intravascular ultrasound (IVUS) images. The main advantage of selective coronary angiography is it provides projectional X-ray images of contrast filled coronary vessels. This enable the vessel lumen to be viewed in detail. However, selective coronary angiography offers no information about the coronary wall.

IVUS imaging offers image information complementary to that provided by angiography. The IVUS imaging generates cross-sectional high resolution images (up to 113 m) of the lumen, plaque, and vessel wall. This characteristic are essential for clinical diagnosis since to date, not many modality enabling the accurate morphological segmentation of the vessel mem-brane and plague in

Published by: The Mattingley Publishing Co., Inc.

March - April 2020
ISSN: 0193-4120 Page No. 7984 - 7992

vivo. The information obtained from the IVUS image can be used for diagnostic purposes such as to facilitate analysis of arteriosclerotic vascular disease [2].

Calcium is a powerful reflector of ultrasound. Only little of the beam enter or penetrates the calcium. Due to that reason, calcium casts a shadow over deeper arterial structures. In IVUS image, Coronary artery calcification (CAC) appear as a bright hyperechoic (echo dense) compared to the adventitia and often appear with a corresponding acoustic shadowing (Figure 1) [3].

The coronary artery calcification is an important marker for coronary artery disease. It is known to correlate with the degree of atherosclerosis and possibly the rate of future cardiac events. The presence or absence of calcium are also shown to be an important determinant of the Percutaneous Coronary Intervention (PCI) success [4]. In addition, cal-cium is also a known limitation of successful directional atherectomy. Whereas extensive calcium is considered con-traindicated, atherectomy is feasible with small, focal areas of calcium [5].

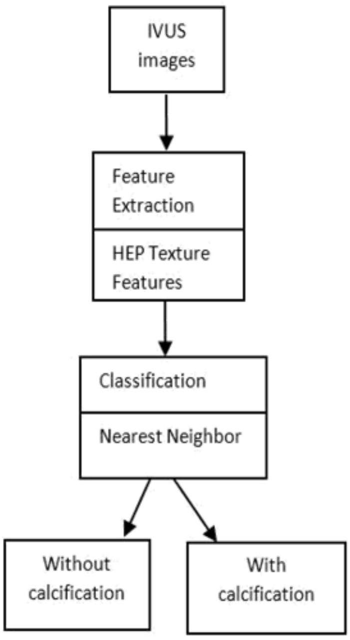

Fig. 1: LEFT: Normal IVUS image

RIGHT: IVUS Image with Calcification. White Arrow indicates the calcification while white indicates the corresponding acoustic shadowing [3].

II. LITERATURE REVIEW

Many works is currently in progress to develop semi-automatic and automatic detection of Coronary artery calcification. Bayesian Classifier [6] and Fuzzy k means [7] are used to find calcification inside the region between lumen and vessel wall, after the detection of lumen and media adventitia borders. Another work is described in [8]. The proposed method start with a segmentation of coronary wall and plaque, followed by determination of plaque composition to one of the main three classes: soft plaque, hard plaque, or hard plaque shadow.

The following two works exploits the fact that the calci-fication regions often represent high intensity echo in IVUS images. This fact makes possible to segment calcified regions by using gray level threshold techniques. Work in [9] used adaptive threshold (Otsu method) because of the intensity level change from image to image, followed by morphological operation and an empirical threshold to detect the boundary of the calcification. Similarly [10] also uses Otsu thresholding and to eliminate wrongly segmented bright regions. Detection of acoustic shadow is also being performed.

Work in [11] detect calcification directly by applying coarse-to-fine strategy to locate the calcification region. The method involved 3 main steps. The first is pixel classification using Rayleigh Mixture Model (RMM) and followed by the detec-tion of Angular Location of the calcification using Markov Random Field (MRF). The second step is the refinement of the detected calcification region by five predefined constraints. Lastly Graph Searching algorithm is used to detect the final calcification border.

Other than segmenting region of interest, calcification is also detected by assessing the overall

Published by: The Mattingley Publishing Co., Inc.

March - April 2020
ISSN: 0193-4120 Page No. 7984 - 7992

appearances of the IVUS image. Using this approach a unique image pattern is extracted from the image and reasoning is made to identify the relationship between the perceived patterns and possible diagnosis. This work has the advantages of not relying on the result of segmentation of other regions. One such work is by [12]. The work used deep learning together with sev-eral well-known classifiers to detect calcification present and calcification absents in an IVUS image.

In this paper we propose a framework for calcification detection using 38 texture descriptors belonging to Histogram of Equivalent Patterns (HEP) Features. A 1-NN classifier were then used as classifier to classify the images into one of these two classes, image with calcification and images without calcification. A 2-fold cross-validation process is applied to a database of 2175 IVUS image to evaluate the performance of the proposed approach.

III. METHODOLOGY

A. Dataset

In this study, we used IVUS images obtain from dataset B of the MICCAI challenge 2011 [13]. All together there are 2175 images in the dataset, all with present of plagues. Out of this 530 shows sign of calcification. The images are obtained from 10 patients and the imaging system used is a Si5 (Volcano Corporation), equipped with a 20 MHz Eagle Eye monorail catheter. It was extracted from in vivo pullbacks of human coronary arteries. These images were in gray scale (255 gray levels), PNG format and with the size of 384 x 384. Somesamples of IVUS images in the dataset are as shown in Figure 2.

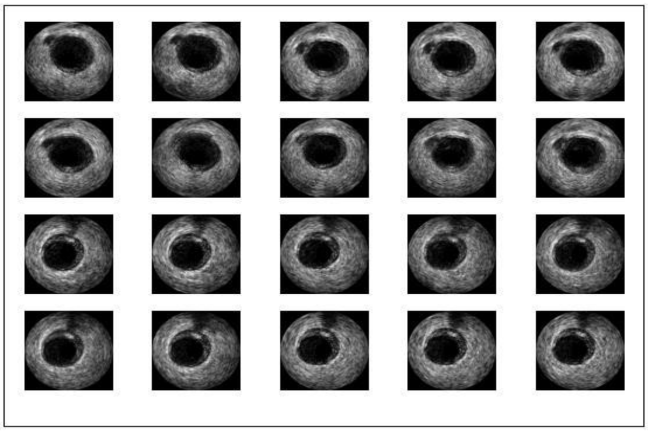

Fig. 2: Some samples of IVUS images

B. Calcification Classification

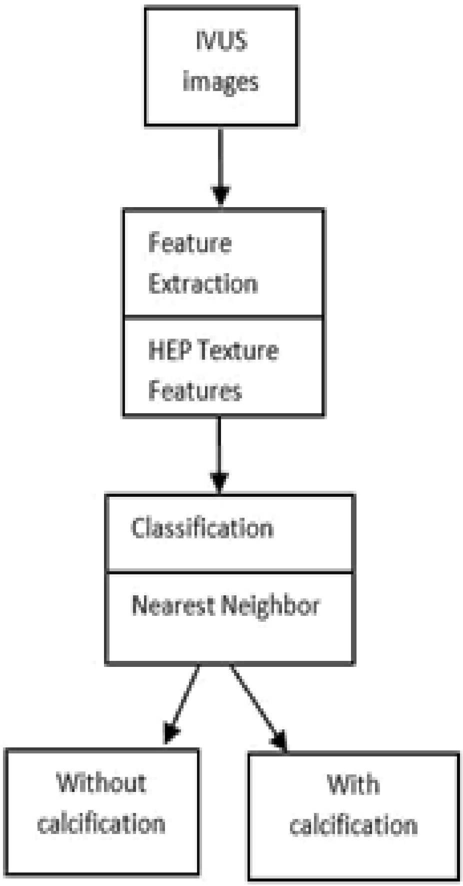

Fig. 3: The framework of the proposed approach

Based on some studies, in IVUS image, calcification regions are usually appear as bright regions in due to its high reflection of the ultrasound beam. Because of that many had assumed that they can be segmented as region of interest (ROI) by thresholding. However, this approach is not very

Published by: The Mattingley Publishing Co., Inc.

accurate and in fact difficult because most often, normal tissue, parts of the catheter, and other artifacts may, also, appear as bright regions in the images. Thus there are possibility that they may be wrongly segmented as one of calcification region [10].

Because of that, rather than performing segmentation on the specific calcification region, we proposed a classification approach. We implement the standard method of classification that is by employing a HEPs feature together with 1-NN classifier with L_1 distance and classify the whole image as either a normal IVUS image without calcification or an IVUS image with calcification. 1-NN classifier is chosen because it is one of the most commonly used classifier to test texture analysis algorithms. Furthermore it can be used without additional tuning parameters. Fig. 3 shows the main elements of our approach and indicates the information flow within the system. Basically it involve taking an IVUS image, followed by feature extraction using HEP features. Then the image will be classified into the two classes mentioned earlier using 1-NN classifier.

C. Histogram of Equivalent Patterns (HEPs)

Histogram of Equivalent Patterns (HEPs) features was first introduced in [14]. HEPs features is a family of texture features descriptors which share the same basic principles, though they have been developed and presented independently in literature. There are 38 texture features descriptors which is categorized as HEPs feature, which are listed in Table I.

Table I: HEPs Features

No	Features g
1	3D Local Binary Patterns (3DLBP)
2	Binary gradient contours 1 (BGC1)
3	Binary gradient contours 2 (BGC2)
4	Binary gradient contours 3 (BGC3)
5	Binary texture co-occurrence spectrum (BTCS+)
6	Centralized binary patterns (CBP)
7	Coordinated clusters representation (CCR)
8	Completed local binary patterns M (CLBP M)
9	Completed local binary patterns MxC (CLBP MxC)
10	Completed local binary patterns S MxC (CLBP S MxC)
11	Completed local binary patterns SxM (CLBP SxM)
12	Completed local binary patterns SxMxC (CLBP SxMxC)
13	Center-symmetric local binary patterns (CS-LBP)
14	Center-symmetric texture spectrum (CS-TSdelta)
15	Improved center-symmetric local binary patterns D (D-LBP)
16	Gradient-based local binary patterns (GLBP)
17	Grey level co-occurrence matrices (GLCM)
18	Grey level differences (GLD)
19	Gray level texture co-occurrence spectrum (GLTCS+)
20	Gradient texture unit coding (GTUC)
21	Improved binary gradient contours 1 (IBGC1)
22	Improved center-symmetric texture spectrum (ICS-TSdelta)
23	Improved center-symmetric local binary patterns (ID-LBP)
24	Improved local binary patterns (ILBP)
25	Improved local ternary patterns (ILTP)
26	Local binary patterns (LBP @ CLBP S)
27	Local quinary patterns (LQP)
28	Local ternary patterns (LTP)
29	Median binary patterns(MBP)
30	Modified texture spectrum(MTS)
31	Rank transform(RT)
32	Reduced texture units(RTU)
33	Sum and difference histograms(SDH)
34	Simplified texture spectrum(STS)
35	Simplified texture units (+) (STU+)
36	Simplified texture units () (STUx)
37	Texture spectrum (TSO)
38	Texture spectrum (TSdelta)

The basic principles shared by all HEPs feature are they are based on neighborhood of predefined shape (rectangular) of fixed size. The rectangular shape is moved along theimage by steps of one pixel. In each position, one among K predefined class label will be assigned to the neighborhood, and the corresponding k th component of feature vector h is incremented by 1=D, where D is the normalizing factor. Therefore the feature vector represents the probability of occurrence of each class (factor 1=D normalizes the feature vector to sum one).

Fernandez et. al. [14] has defined the HEP descriptor as inEquation 1 and Equation 2 as follows:

Definition 1:

A texture descriptor HEP is defined as a function F that receives an image I and return a feature vector h. I is an M xN matrix representing the pixel

March - April 2020
ISSN: 0193-4120 Page No. 7984 - 7992

intensities of an image quantize to G grey levels. $I_{m;n}$ is the grey-scale intensity at pixel (m; n).

h = F (I)

Definition 2:

the k th element of h is expressed as follow:

^{m}max ^{n}max

$m=m_{min}$ $n=n_{min}$

where:

– m and n = represent row and column-wise pixel indices,

– $x_{m;n}$ = the grey scale values of a set of pixels defining a generic neighborhood $_{m;n}$ around (m; n),

– = a vector of parameters computed from the whole image

– D = normalizing factor

– f = a generic function that returns an integer between 0 and K 1.

$h_k = (1=D) X \quad ^{X} [f(x_{m;n};) \; k]$

– = defined as Equation 3

$(x) =^{1x = 0}$ (3)

otherwise

The list the 38 HEP feature descriptors is in Table I. Some of the HEP features will be briefly explained in the following subsection. For detail description of other descriptors, kindly refer to [14].

1) Binary gradient contour: Binary gradient contour (BGC)is a family of descriptor based on pairwise comparisonof adjacent pixels belonging to one or more closed path traced along the periphery of the 3x3 neighborhood. There are there type of BGC, depending on the closed path selected. They are called BGC1, BGC2 and BGC3. Improved Binary gradient contour1 is an extension of BGC1. With IBGC1, a central pixel is introduced and the comparison is conducted between the central pixels and average gray scale value.

2) Texture spectrum: Texture spectrum, introduced by He and Wang [16] characterize local texture information in all

eight directions. The method is said as the precursor for a set of more recent method such as Local Binary Pattern (LBP). In Texture spectrum , each peripheral pixel in the3x3 neighborhood is assigned a value 0, 1, or 2 if its grey level intensity is less, equal or greater that the central pixel respectively. Texture spectrum is an advancement of the method Texture spectrum , whereby they are made to be more robust to the presence of noise by introducing a threshold value above zero.

3) Local Ternary Pattern: Local Ternary Pattern (LTP)

[17] is a hybrid between texture spectrum and local binary patterns. The main similarity between the methods is the used of thresholding. However unlike LBP, LTP does not threshold the pixels into 0 and 1, rather it uses a threshold constant to threshold pixels into three values, just like texture spectrum. Improved LTP (ILTP) [18] is the improved version of LTP, which is designed to make the method more robust to the presence of noise. In ILTP each pixel in the neighborhood is thresholded at the average gray scale value.

4) Completed Local Binary Pattern: Completed Local Bi-nary Pattern (CLBP) is introduced by [19] and it is an extension of LBP. In CLBP, a local region is represented by its center pixel and a Local Difference Sign-Magnitude Transform (LDSMT). The center pixel is simply coded by a binary code after global thresholding, and the binary map is named as CLBP Center (CLBP C).

The LDSMT decomposes the image local structure into two complementary components: the difference signs (CLBP S) or the original LBP and the difference magnitudes (CLBP M). All the three code

Published by: The Mattingley Publishing Co., Inc.

March - April 2020
ISSN: 0193-4120 Page No. 7984 - 7992

maps, CLBP C, CLBP S and CLBP M, are in binary format so that they can be readily combined to form the final CLBP histogram. All approaches of CLBP applied in this experiment are based on different combination of these three basic descriptors: CLBP S, CLBP C and CLBP M.

For example, CLBP MxC is obtained by calculating the 2D joint histogram of CLBP M and CLBP C and CLBP SxM is obtained by calculating the 2D joint histogram of CLBP M and CLBP S, CLBP SxMxC is obtained by calculating the 3D joint histogram of CLBP S, CLBP M and CLBP C and CLBP S MxC is obtained by first calculating a joint 2D his-togram of CLBP C and CLBP M, then converting it into ID histogram and then concatenated it with CLBP S to generate the final joint histogram.

IV. EXPERIMENTAL RESULT

The experiment was conducted using all images in the dataset. The classification is a 2-class classification: classifying an image as one of two types, a normal image (no calcification) or an image with calcification. 2-fold cross validation is used by randomly selecting half of the images for training and the remaining half for testing.

The experiment is repeated four times, each time with a different subdivision of training and test set. The mean recognition rate (mean accuracy) over the four run, standard deviation, extraction time and recognition time for each tex-ture features are recorded and will be used to compare the performance of each HEPs feature descriptors. The extraction time is the time of feature extraction for all the test images and the recognition time is the time of recognition for all the test images.

Table II: Performance of the HEP Features

No	Features	Mean Acc	Std	Extraction Time (s)	Recognition Time(s)
1	3DLBP	92.92	0.86	262.92	2.42
2	BGC1	93.50	0.85	70.49	0.79
3	BGC2	93.45	0.7	66.99	0.84
4	BGC3	93.64	0.87	68.49	0.74
5	BTCS+	85.8	0.71	50.78	0.39
6	CBP	89.20	1.07	53.23	0.25
7	CCR	89.04	0.66	91.15	1.67
8	CLBP M	89.02	0.47	78.42	0.96
9	CLBP MxC	**94.09**	0.9	91.19	1.56
10	CLBP S MxC	**95.11**	0.09	131.35	2.0
11	CLBP SxM	**94.49**	0.99	158.90	207.97
12	CLBP SxMxC	**95.89**	0.40	190.65	548.59
13	CS-LBP	87.78	1.04	45.89	0.73
14	CS-TSdelta	92.35	0.73	65.76	0.39
15	D-LBP	88.47	1.01	41.58	0.35
16	GLBP	87.75	0.89	97.8	1.9
17	GLCM	92.76	0.59	222.96	154.36
18	GLD	83.62	0.91	70.31	0.97
19	GLTCS+	90.63	0.47	109.98	0.3
20	GTUC	90.40	1.27	109.99	8.75
21	IBGC1	94.55	0.71	105.67	1.84
22	ICS-TSdelta	90.85	0.55	75.93	0.39
23	ID-LBP	84.21	1.05	35.35	0.22
24	ILBP	93.89	0.92	85.03	2.72
25	ILTP	94.23	0.78	148.64	2.29
26	LBP @ CLBP_S	92.85	1.19	72.77	0.97
27	LQP	91.93	0.49	146.84	2.04
28	LTP	93.59	1.07	102.47	1.41
29	MBP	92.19	0.68	126.3	1.18
30	MTS	89.22	0.76	38.95	0.45
31	RT	84.15	0.77	30.16	0.24
32	RTU	89.32	0.83	37.78	0.35
33	SDH	93.20	0.83	137.24	7.43
34	STS	92.85	0.99	45.82	0.48
35	STU+	92.21	0.84	53.33	0.42
36	STUx	93.04	0.9	78.64	0.89
37	TSO	95.31	0.93	104.75	13.8
38	TSdelta	94.26	0.76	113.79	12.64

The results is as Table II. Based on the Table II, the mean accuracy obtained from all descriptors are between 83.62% to 95.89%. From the result, the following observation can be made. First The top performer descriptors with mean accuracy above 94% are obtained through the use of Improved binary gradient contour 1 (IBCG1), Completed local binary patterns MxC (CLBP MxC), Completed local binary pattern S MxC (CLBP S MxC), Completed local binary patterns SxM (CLBP SxM), Completed local binary patterns SxMxC (CLBP SxMxC), Improved local ternary patterns (ILTP), Tex-ture spectrum (TSO) and Texture spectrum (TSdelta). Basically we can say the best descriptors in this experiment are a variant of Completed Local Binary Pattern (CLBP), Texture Spectrum (TS), Local Ternary Pattern (LTP) and Improved Binary Gradient Contour (IBGC).

Second, ILTP obtained better result than LTP with a mean accuracy of 94.23% and 93.58% respectively. This is as expected as ILTP is the improved variant of LTP. Similar ob-servation can be made with BGC variant. IBGC1 outperformed BCG1 with a mean

Published by: The Mattingley Publishing Co., Inc.

March - April 2020
ISSN: 0193-4120 Page No. 7984 - 7992

accuracy 94.55% and 93.50% respectively. For Texture Spectrum variant the result is not as we expected. TSO performed better with 95.31% than TSdelta with 94.26%.

Third, normal LBP (or CLBP S) obtained higher recogni-tion rate as compared to CLBP M with a mean accuracy of 92.85% and 89.02% respectively. This re-confirm the finding made in [19] that the sign component (CLBP S) preserves more image local structural information than the magnitude component (CLBP M), thus enable the CLBP S operator to obtain better result than CLBP M for texture classification.

The result also show that the fusion of CLBP features improves the recognition rate. For example CLBP MxC and CLBP SxM show better result as compared to the result of CLBP S and CLBP M individually. The fusion of three CLBP features namely CLPB S MxC and CLBP SxMxC also show better result than the CLBP with the fusion of only two CLBP features. This is because each CLBP component contains complementary features, thus by fusion them together either jointly or in concatenation, better recognition was obtained. The result also shows that CLB SxMxC obtained slightly higher mean accuracy as compared to CLBP S MxC, however it should be noted that the dimension of the CLBP SxMxC is larger, which resulted in a longer time required for feature extraction and classification.

If we compare LTP and Texture spectrum with CLBP we can see that the result of ILTP and TS is better when compared to individual element of CLBP i.e. CLBP S and CLBP M. This is because ILTP and Texture Spectrum is designed to be more robust to noise as compared to CLBP M and CLBP S. In addition, in ILTP and Texture Spectrum, the local difference is quantized into three difference level, while for each component CLBP it is quantized into only two levels.

If we compared the fusion of CLBP, then the result of CLBP is better. Both CLBP S MxC and CLBP SxMxC show better performance as compared to IBGC1 and ILTP descriptors. Thereason is as mentioned earlier, i.e. fusion CLBP will have complementary features which will make the descriptors more robust for texture classification.

As for Texture Spectrum, CLBP SxMxC perform better, however CLBP S MxC show slightly less mean accuracy as compared to TSO with a mean accuracy of 95.11% and 95.31% respectively. It is worth pointing out that although mean accuracy for CLBP S MxC is lower but the standard deviation for CLBP S MxC is lower compared to TSO. A lower standard deviation indicates that the data points to be closer to the mean or expected value, while a higher standard deviation indicates that the data points are more spread out over a wider range of value. This show that CLBP S MxC mean accuracy is more consistent and does not vary a lot as compared to the TSO descriptors.

The extraction time and the recognition time for all descrip-tors are acceptable. All the best performers descriptors requires less than 160s of extraction time to extract the features with the exception of CLBP SxMxC, which takes 191s of extraction time. Similarly, the highest recognition time is CLBP SxMxC. This is because the feature vector for CLBP SxMxC is larger, thus it use more extraction and recognition time as comparedto other features which is of lower dimension.

Table III: Comparison with other methods

Methods	No of Images	Result
dos Santos Filho, Esmer-aldo, et al [10]	20 IVUS images, 15 with calcification and 5 without calcification	Sensitivity = 84%, Specificity = 88%, AUC = 0.87
Gao, Zhifan, et al. [11]	996 IVUS image, 498 with calcified plague and acoustic shadowing and 498 without calcified plague but with no acoustic shad-owing	Sensitivity = 94.68%, Specificity = 95.82%
Sofian, Hannah, et al. [9]	100 IVUS images, 50 with calcified plague and 50 without calcified plague.	Sensitivity = 80%, Specificity = 84%, Accuracy = 82%
Sofian, Hannah, et al. [12]	2175 IVUS images, 530 with calcification and 1645 without calcification.	Sensitivity = 98%, Specificity = 99%, Accuracy = 99%
Proposed	2175 IVUS images, 530 with calcification and 1645 without calcification.	Accuracy = 95.89%
Taki, Arash, et al. [6]	60 IVUS images, 30 with calcification and 30 without calcification.	Sensitivity = 92.67%, Specificity = 98.5%, Area under curve= 94.3%

Published by: The Mattingley Publishing Co., Inc.

Table III show the performance comparison of the proposed approach and other methods. From the table we can see that the method performed reasonably well with a highest accuracy of 95.89

V. CONCLUSION

In this paper we classify IVUS images into two classes, an IVUS image with Calcification presence or an IVUS image without Calcification presence. We used 38 features from HEP features descriptors and compared their mean accuracy, recognition time and extraction time. The result demonstrates IVUS images can be classified into two separate classes using HEP features. The result also show that CLBP SxMxC obtained the highest mean accuracy as compared to other methods. Future work will be evaluating the method with a data set and with more variation of IVUS image classes. classification.

REFERENCES

[1] "World health statistics 2018: Monitoring health for the sustainabledevelopment goal (sdgs)," 2018, accessed: 2019-04-30. [Online].Available:https://www.who.int/gho/publications

[2] M. E. Plissiti, D. I. Fotiadis, L. K. Michalis, and G. E. Bozios, "An automated method for lumen and media-adventitia border detection in a sequence of ivus frames," IEEE Transactions on Information Technology in Biomedicine, vol. 8, no. 2, pp. 131–141, 2004.

[3] G. S. Mintz, "Intravascular imaging of coronary calcification and its clinical implications," JACC: Cardiovascular Imaging, vol. 8, no. 4, pp. 461–471, 2015.

[4] S. K. Sharma, Y. Vengrenyuk, and A. S. Kini, "Ivus, oct, and coronary artery calcification: Is there a bone of contention?" 2017.

[5] D. S. Scott, U. K. Arora, A. Farb, R. Virmani, and N. J. Weissman, "Pathologic validation of a new method to quantify coronary calcific deposits in vivo using intravascular ultrasound," The american Journal of cardiology, vol. 85, no. 1, pp. 37–40, 2000.

[6] A. Taki, Z. Najafi, A. Roodaki, S. K. Setarehdan, R. A. Zoroofi,Konig, and N. Navab, "Automatic segmentation of calcified plaques and vessel borders in ivus images," International Journal of Computer Assisted Radiology and Surgery, vol. 3, no. 3, pp. 347–354, Sep 2008. [Online]. Available: https://doi.org/10.1007/s11548-008-0235-4

[7] N. Dey, A. B. Roy, P. Das, A. Das, and S. S. Chaudhuri, "Detection and measurement of arc of lumen calcification from intravascular ultrasound using harris corner detection," in 2012 NATIONAL CONFERENCE ON COMPUTING AND COMMUNICATION SYSTEMS. IEEE, 2012, pp. 1–6.

[8] X. Zhang, C. R. McKay, and M. Sonka, "Tissue characterization in in-travascular ultrasound images," IEEE Transactions on Medical Imaging, vol. 17, no. 6, pp. 889–899, 1998.

[9] H. Sofian, A. Ng, J. Than, S. Mohamad, and N. M. Noor, "Calcification boundary detection in coronary artery using intravascular ultrasound images," in TENCON 2017-2017 IEEE Region 10 Conference. IEEE, 2017, pp. 2835–2839.

[10] E. Dos Santos Filho, Y. Saijo, A. Tanaka, T. Yambe, S. Li, andYoshizawa, "Automated calcification detection and quantification in intravascular ultrasound images by adaptive thresholding," in WorldCongress on Medical Physics and Biomedical Engineering 2006.Springer, 2007, pp. 1421–1425.

[11] Z. Gao, W. Guo, X. Liu, W. Huang, H. Zhang, N. Tan, W. K. Hau, Y.-Zhang, and H. Liu, "Automated detection framework of the calcified plaque with acoustic shadowing in ivus images," PloS one, vol. 9, no. 11, p. e109997, 2014.

[12] H. Sofian, J. C. M. Than, S. Mohammad, and N. M. Noor, "Calcification detection of coronary artery disease in intravascular ultrasound image: Deep feature learning approach," International Journal of Integrated Engineering, vol. 10, no. 7, 2018.

[13] S. Balocco, C. Gatta, F. Ciompi, A. Wahle, P. Radeva, S. Carlier,Unal, E. Sanidas, J. Mauri, X. Carillo et al., "Standardized eval-uation methodology and reference database for evaluating ivus image segmentation," Computerized medical imaging and graphics, vol. 38,no. 2, pp. 70–90, 2014.
[14] A. Fernandez,´ M. X. Alvarez, and F. Bianconi, "Texture description through histograms of equivalent patterns," Journal of mathematical imaging and vision, vol. 45, no. 1, pp. 76–102, 2013.
[15] A. Fernandez, M. X. Alvarez, and F. Bianconi, "Image classification with binary gradient contours," Optics and Lasers in Engineering, vol. 49, no. 9-10, pp. 1177–1184, 2011.
[16] L. Wang and D.-C. He, "Texture classification using texture spectrum," Pattern Recognition, vol. 23, no. 8, pp. 905–910, 1990.
[17] X. Tan and W. Triggs, "Enhanced local texture feature sets for face recognition under difficult lighting conditions," IEEE transactions on image processing, vol. 19, no. 6, pp. 1635–1650, 2010.
[18] L. Nanni, S. Brahnam, and A. Lumini, "A local approach based on a local binary patterns variant texture descriptor for classifying pain states," Expert Systems with Applications, vol. 37, no. 12, pp. 7888– 7894, 2010.
[19] Z. Guo, L. Zhang, and D. Zhang, "A completed modeling of local binary pattern operator for texture classification," IEEE transactions on image processing, vol. 19, no. 6, pp. 1657–1663, 2010.